Lattice Boltzmann simulation on the flow behaviour associated with Helmholtz cavity-backed acoustic liners

J. Heng, T.D. Thanapal, W.L. Chan* and B. Elhadidi

School of Mechanical and Aerospace Engineering, Nanyang Technological University
50 Nanyang Avenue, Singapore 639798, Singapore

Abstract

Noise from jet engines can be reduced by means of a Helmholtz cavity configuration. The resonance that occurs when a flow passes the neck of the Helmholtz resonator will dissipate acoustical energy. The mechanism for such dissipation is mainly due to the vortex shedding that occurs at the neck of the resonator where the vortex structures absorb acoustical energy and subsequently dissipate through viscous effects. In this work, numerical simulations utilizing the Lattice Boltzmann method is used to aid in visualizing the flow behaviour that is associated with Helmholtz cavity-backed acoustic liners. In both experiments and numerical simulations, the 1-neck cavity is found to result in an amplification of an applied acoustic source. For a 4-neck cavity, the configuration is able to achieve acoustic pressure reductions. Differences in the flow behaviour of the 1-neck and 4-neck cavities are detailed in this work. Results show that stronger vortex shedding that occurs in the 4-neck cavity configuration could explain the increased effectiveness of a Helmholtz cavity-backed acoustic liner.

Keywords: Aeroacoustics, Lattice Boltzmann method, Acoustic liner, Helmholtz resonator
*Corresponding author: chan.wl@ntu.edu.sg, Tel: +(65) 67904861

Acknowledgements

Funding for this project is provided by the National Research Foundation, Singapore (NRF2016NRF-NSFC001-102). The authors are grateful for the computing resource allocated by National Supercomputing Centre, Singapore and the support from its staff. The authors are also grateful for the input of T.Y. Ng and T.H. New to the project.

1 Introduction

Noise, more often than not, is perceived as a nuisance and sometimes even detrimental to health. Examples of such unwanted noise can be from combustion jet engines operating at a nearby airport, or from loud engine pipes of fast-moving cars across highways in urban built-up areas. Noise can also occur within a car when its window is wound down while it is moving. This is a result when air blows past an orifice (open car window) of a cavity (interior of the car) where it generates a resonance with uncomfortable pressure fluctuations inside the car. Such is an example of a Helmholtz resonator at work. In the car, this may be an unwanted phenomenon. However, resonance from a Helmholtz resonator can be designed to help reduce some of the unwanted noise generated by those of a jet engine mentioned above.

Early work has been performed to investigate the use of Helmholtz resonators in reducing acoustic fluctuations. Meyer, Mechel, & Kurtze (1958) found that for a grazing flow across the Helmholtz resonator opening, an increase in the velocity of grazing flow decreases its effectiveness in sound attenuation. They have also demonstrated that under certain conditions of an undamped Helmholtz resonator (where all walls of the cavity are hard walls), a negative attenuation (or amplification) may occur. Looking within the cavity, Ma, Slaboch, & Morris (2009) presented a framework to predict the pressure fluctuations inside a Helmholtz resonator cavity. Subsequently, this could be used to study its effects on the resonant frequency of the resonator which is arguably important for the design for acoustical damping systems that utilize the Helmholtz resonator configuration. More importantly, Eldredge & Dowling (2003) detailed that a periodical shedding of vorticity from an orifice works to absorb acoustical waves by the transfer of acoustic energy into vortical energy of the shedding. This energy is subsequently dissipated. The finding is significant such that these vortex sheddings are later observed in the simulations of the current work and helps provide a basis for current analyses. More recent work includes that of Tam, Pastouchenko, Jones, & Watson (2014) who worked to improve understanding of perforated acoustic liners. They found that in a grazing flow configuration, a feedback acoustic resonance mechanism is present and such mechanism also introduces additional drag on top of a turbulent boundary layer drag from flow over a flat wall. Then, Stein, Reiss, & Sesterhenn (2018) looked at how the grazing flow-Helmholtz resonator configuration affects the turbulent boundary layer by means of Direct Numerical Simulation. These works present some visualization of the flow associated with the Helmholtz cavity but focus on the turbulence that happens around the neck. Other configurations of the grazing flow-Helmholtz cavity case have also been recently looked at; however, such structures have to deal with more variables and much work still has to be done on investigating many of the configurations possible. One such example is that of the work of Zhao, Ang, & Ji (2015) who looked at the properties of perforated liners and its damping behaviour in both single-layer and double-layer configurations.

Recognizing that most of the previous work has mainly focused on conventional Helmholtz resonators with one neck and its associated effects, the focus in this paper is placed on considering that a multiple-neck resonator configuration is different from a single-neck configuration. Such a multiple-neck configuration is more akin to Helmholtz resonators with perforated liners (Zhao, Ang, & Ji, 2015; Jing & Sun, 2000), which were generally studied with the assumption that the liner orifices act independently of each other. Here, the assumption of independent orifices is relaxed such that multiple necks are now thought to interact with each other in the presence of a grazing flow and such interactions may result in enhanced acoustical dissipation. Lattice Boltzmann method (LBM) is chosen as it is a highly parallelizable computational method that is capable of high-fidelity simulations. A short description of the LBM is first presented, followed by a description of the numerical setup used in the study. Instantaneous snapshots of the simulations will then provide insights the flow behaviour associated with the 1-neck and 4-neck cavity configurations.

2 Lattice Boltzmann Method

The description of fluid in the LBM is through the use of distribution functions which tracks the 'number' of fluid particles present in a certain fluid cell (lattice). This particle distribution function f contains information on time and physical space. In addition to that, it is also a function of velocity space. The velocity space provides information on the direction of the particles' velocity. The particle distribution function is written as $f(\boldsymbol{x}, \boldsymbol{\xi}, t)$, where $\boldsymbol{x}$ is the three-dimensional physical space (x, y, z), $\boldsymbol{\xi}$ is the three-dimensional velocity space (ξ_x, ξ_y, ξ_z) and t is time. In other words, the distribution function $f(\boldsymbol{x}, \boldsymbol{\xi}, t)$ is the density of particles with velocity $\boldsymbol{\xi}$ at position $\boldsymbol{x}$ and time t. To recover the macroscopic fluid properties, moments of the distribution functions, which are the integral of the distribution functions weighted by functions of $\boldsymbol{\xi}$, are obtained. The first moment of the distribution function is:

$$\rho(\boldsymbol{x}, t) = \int f(\boldsymbol{x}, \boldsymbol{\xi}, t) d^3\xi \quad (1)$$

where the distribution function is integrated over all possible velocities at a certain space and time to obtain the density ρ. Likewise, the fluid velocity can be obtained by:

$$\rho(\boldsymbol{x}, t)\boldsymbol{u}(\boldsymbol{x}, t) = \int \boldsymbol{\xi} f(\boldsymbol{x}, \boldsymbol{\xi}, t) d^3\xi \quad (2)$$

When two particles collide, a range of scenarios can happen. For example, they could have a head-on collision and go back in their respective directions where they came from. They could also collide in such a way that they bounce off at right angles to the direction they came from. Lastly, they could just lightly graze each other and continue forwards in the same direction they were travelling. Now consider a lattice space where there are many particles and such collisions are constantly taking place. The collisions will cancel out and the distribution functions in that lattice site will reach an equilibrium distribution which can be written as:

$$f^{eq}(\boldsymbol{x}, |\boldsymbol{v}|, t) = \rho \left(\frac{1}{2\pi RT}\right)^{\frac{3}{2}} e^{-\frac{|v|^2}{2RT}} \tag{3}$$

where R is the universal gas constant and T is the temperature. The Boltzmann equation is a form of transport equation for the distribution functions and the force-free Boltzmann equation reads:

$$\frac{\partial f}{\partial t} + \xi_\beta \frac{\partial f}{\partial x_\beta} = \Omega(f) \tag{4}$$

where the summation convention is used and $\Omega(f)$ is a collision operator. Over time, the collision of particles tends to 'relax' the distribution functions to the equilibrium function. This relaxation is captured by the collision operator in equation 4. The collision operator can take many forms depending on the properties of the fluid flow. However, the simplest and most commonly used collision operator is the Bhatnagar, Gross and Krook (BGK) operator:

$$\Omega(f) = -\frac{1}{\tau}(f - f^{eq}) \tag{5}$$

where τ is the relaxation time. To implement a force-free Boltzmann equation (equation 4) in numerical simulations, the equation is discretized in velocity space, physical space and time to give:

$$f_i(\boldsymbol{x} + \boldsymbol{c}_i \Delta t, t + \Delta t) = f_i(\boldsymbol{x}, t) + \Omega_i(\boldsymbol{x}, t) \tag{6}$$

where $\boldsymbol{c}_i$ is the velocity sets. Equation 6 is called the lattice Boltzmann equation. Complete with the BGK collision operator, the discretized equation is:

$$f_i(\boldsymbol{x} + \boldsymbol{c}_i \Delta t, t + \Delta t) = f_i(\boldsymbol{x}, t) - \frac{\Delta t}{\tau}\left(f_i(\boldsymbol{x}, t) - {f_i}^{eq}(\boldsymbol{x}, t)\right) \tag{7}$$

where the discretized equilibrium function is:

$${f_i}^{eq}(\boldsymbol{x}, t) = w_i \rho \left(1 + \frac{\boldsymbol{u} \cdot c_i}{{c_s}^2} + \frac{(\boldsymbol{u} \cdot c_i)^2}{2{c_s}^4} - \frac{\boldsymbol{u} \cdot \boldsymbol{u}}{2{c_s}^2}\right) \tag{8}$$

where w_i is the weight function and c_s is the lattice speed of sound. A more detailed description of the LBM is available in Sukop & Daniel T. Thorne (2006).

3 Simulation Setup

3.1 Domain description

The simulation domain will be modelled after an impedance tube experimental rig set up on-site as a means to validate some of the results. Figure 1 shows a schematic of the impedance tube, which is $2.5m$ in length (inclusive of the liner and excluding the air pump). The tube is a square channel ① with a cross-sectional dimension of $0.05m \times 0.05m$ and consists of an air pump ②, a speaker ③, an acoustic liner ④, and four independent cavities ⑤. Microphones ⑥ are fixed on one of the faces of the impedance tube wall. The blower is attached at the inlet to provide a grazing flow in the tube at about $20m/s$. The speaker is placed $0.4m$ downstream of the inlet as the acoustic source. A tonal frequency of $300Hz$ is used in both the experiments and simulations. The acoustic liner is located at about $1.4m$ from the inlet and are of the same cross-sectional dimension as the impedance tube. The perforations on the liners connect the impedance tube to the cavity which will act like Helmholtz resonators. The cavity is a rectangular cuboid of dimensions $0.1m \times 0.08m \times 0.04m$. The liner can be swapped out of the impedance tube to investigate liners with different perforation configurations. The numerical simulation domain shown in Figure 2 is modelled according to the experimental setup. The domain schematic shown is that for a liner with one orifice. This paper will mainly focus on two liner configurations – a single orifice and four orifices, each of the same dimensions as the single orifice liner. Each orifice has a dimension of $0.01m \times 0.01m$ and is $0.01m$ deep. Figure 3 shows the configuration of the orifices simulated.

Figure 1 Schematic of the impedance tube experimental rig. Drawing not to scale, dimensions in mm.

Figure 2 Simulation domain modelled according to the experimental rig fixed with an acoustic liner with one orifice. Drawing not to scale, dimensions in mm.

Figure 3 Isometric models of the 1-neck (left) and 4-neck (right) cavity where four identical parts are combined to make a square cross-sectioned acoustic liner.

3.2 Numerical scheme and boundary conditions

The numerical simulation is performed using the open-source LBM code package Palabos. The most commonly used D3Q19 velocity set is used in the study. For the collision operator in equation 4, the simplest BGK collision operator is used as it is sufficient to simulate a behaviour akin to the compressible Navier-Stokes equation. The Smagorinsky turbulence model with a model constant of 0.1 is also applied. The above numerical scheme has been previously shown to perform adequately compared to a DNS of channel flow (Gehrke, Janßen, & Rung, 2017).

At the impedance tube inlet, an inlet velocity of $20m/s$ with a turbulence intensity of 0.3% is applied in accordance with measurements obtained from the experimental rig. Next, at the tube outlet, a first-order non-reflecting outlet is applied to reduce acoustical reflections from the open end. Its implementation is by simply overwriting the population distribution functions at the last column of the tube with those from the penultimate column. This implementation is favoured over the second-order implementation as the latter involves finite difference approximations over three columns of lattice and would also result in a loss of the LBM's advantage of having all operations occurring locally at each lattice. A second-order implementation will also negatively impact the simulation time required. The acoustic source is being applied through a sinusoidally varying velocity inlet and the amplitude of the velocity is obtained using the equation $p = \rho_0 cu$ (Kinsler, Frey, Coppens, & Sanders, 1999).

3.3 Lattice dependency tests

A series of lattice dependency tests is first performed. The velocity flow profile within the impedance tube is first obtained by traversing a hot wire anemometer across the outlet of the impedance tube. The velocity profile is compared against simulation results from three different lattice resolutions – $N = 50$, 100, and 150, where N is the number of lattice divisions in the spanwise direction of the impedance tube ($0.05m$). Figure 4 plots the fully developed velocity profile of the flow at the impedance tube outlet, without a cavity, for three different lattice resolutions and that for experimental measurements obtained. The corresponding y+ of the first lattice from the wall is also indicated. The flow profile of $N = 100$ and 150 matches closely to the experimental measurements as expected from the numerical scheme used. However, $N = 50$ shows a slight deviation with about 5% error. As the computational cost of LBM required is linearly proportional to the lattice size (Krüger et al., 2017), the computational resource required for $N = 50$ is about an eighth of that of $N = 100$.

Next, for the purpose of dependency test, a tonal frequency of 300Hz is applied as a velocity boundary condition at the acoustic inlet. The velocity amplitude is prescribed such that the eventual acoustic wave has a sound pressure level (SPL) of 120dB. Acoustic pressure is obtained from a location downstream corresponding to the location of one of the microphones in the experiments. By passing the pressure data through Fast Fourier Transform (FFT), the tonal frequency is then recovered, as shown in Figure 5. It is seen that for both resolutions ($N = 50$ and 100) tested, the SPL recovered for the $300Hz$ signal in both cases are in excellent agreement with each other. Since both grid resolutions perform similarly, $N = 50$ is chosen for simulations where the recovery of acoustic pressure is of primary. This will aid in greatly reducing the total computational resources required for the entire project. For simulations where flow visualizations are required, for instance in the vicinity of the cavity orifices (mainly those presented in this paper), $N = 100$ is used to allow for higher quality visualizations.

Figure 4 Lattice dependency test of flow profile in the impedance tube for three different lattice resolutions, compared against experimental measurements.

Figure 5 Lattice dependency test of a tonal frequency of $300Hz$ for two different lattice resolutions.

4 Results and Discussions

4.1 Single-neck and multi-neck cavities

Numerical simulations are performed on the two liner configurations shown in Figure 3 (on the $N = 50$ grid) and compared against experimental results. The downstream pressure is measured and FFT is performed on the set of data to assess the effects of the Helmholtz resonator configuration on the $300Hz$ input acoustic signal. Table 1 shows the results of the acoustic pressure normalized against results from the case without liners (i.e. hard-wall across the whole impedance tube).

Table 1 Normalized acoustic pressure of the 300Hz tone downstream of the liner

One observation from Table 1 is that the numerical simulations do not exactly replicate the relative values of acoustic pressure as measured in the experiments. However, this apparent inaccuracy is expected since acoustic pressure fluctuations are very small compared to aerodynamical values. Here, the fluctuations are about four orders of magnitude lower, which would have been much more susceptible to numerical errors. The resolution of these discrepancies between the numerical and experimental results may be achieved by a systematic investigation of the lattice relaxation time, τ, but is beyond the scope of this paper and hence not considered.

Besides, despite the quantitative differences between the numerical and experimental results, the simulations are in fact able to capture the trends that are observed in the experiments. For instance, both numerical and experimental results show an amplification of the acoustic signal downstream of the 1-neck cavity by approximately 25% and 50%, respectively. Clearly, this amplification is opposite of the typical function of a single-neck Helmholtz resonator. In contrast, the 4-neck cavity shows an approximately 50% reduction in the acoustic pressure from its 1-neck counterpart for both the numerical and experimental results. With the qualitative agreements between the numerical and experimental datasets, the simulations can therefore be justifiably used to gain some insights through flow visualizations of both the single- and multi-neck cavities, as discussed in the next section.

4.2 Visualization of flow associated with a Helmholtz cavity

Figure 6 show the lengthwise cross-section of the impedance tube with a 1 and 4-neck cavity at various instants of one $300Hz$-period. The grazing flow is applied upstream from the left to the right (in the figure) and a $300Hz$ acoustic source is also introduced upstream. The two figures lay out, in a side-by-side comparison, of the normalized v velocity (the velocity component that moves in and/or out of the cavity) for one cycle, with the time T denoted by periods of a $300Hz$ wave. The times are representative of the acoustic source occurring at the same moment in time (i.e. coherent). For a clearer depiction of the vortex shedding, insets that focus on the vicinity of the cavity neck have been included for all snapshots.

From here, a few observations can be obtained to aid in the understanding of why a multi-neck cavity perform better in reducing the $300Hz$ acoustic source than a single-neck cavity. Firstly, the vortex shedding that occurs in the 1-neck cavity is much weaker than that seen in the 4-neck cavity. In the 1-neck cavity, the shedding is almost difficult to spot, which can be vaguely seen at $4.00T$ and $4.75T$, where a small volume of air is seen as moving downwards into the impedance tube (see arrow at the inset). Then, it rapidly disappears, and the structure is no longer discernible in the next frame. This insignificant vortex shedding characteristic suggests that a single-cavity configuration is not ideal in achieving acoustical reductions.

For the 4-neck cavity case, the shedding is much more distinguishable and longer-lived. The shedding of a small volume of air moving out of the cavity (indicated by an arrow at the insets) can be seen to start at $4.50T$. This vortex then maintains its structure through $4.75T$ to $5.00T$, where it can be seen convecting past the downstream neck. Since such shedding is previously found to be responsible for the dissipation of acoustical energy, it follows that a stronger and longer-lived vortex should perform better in achieving acoustical reductions. What remains next is to determine a possible cause of such stronger vortex shedding.

Figure 6 Comparison of the normalized vertical velocity (v) associated with a 1-neck (left column) and 4-neck cavity (right column). Grazing flow direction from left to right. Time in periods of $300Hz$. The vortex shedding in both cases is indicated by an arrow in the insets, which focus on the vicinity of the cavity neck(s) that is demarcated by the dashed box. For a better visualization, the readers can refer to the media files attached. However, note that the colour scaling used is different from that shown here.

Figure 7 plots the velocity components that were obtained at the centre of both the upstream and downstream necks of the 4-neck cavity configuration for about five periods. To separate the velocity signal into its corresponding low- (top) and high-frequency (bottom) components, post-processing with a low- and high-pass filter, respectively, were performed. The velocities from $4.00T$ to $5.00T$ corresponds to the instantaneous velocity plots in Figure 6.

In general, the upstream and downstream velocities are seen to be out-of-phase for the low-frequency waves, which were found to be of the same frequency as the signal of $300Hz$, but in-phase for the high-frequency components (i.e. harmonics of $300Hz$, in steps of $600Hz$). Specifically, the phase-shift in the low-frequency velocity components of the upstream and downstream necks were found to be approximately $1.2\pi\ rad$, indicating that the two profiles are coupled with a negative correlation.

A possible attribution for this observation is that multiple necks provide additional pathways connecting the impedance tube to the Helmholtz cavity, which may result in a less restrictive volume within the cavity itself. Then, the whole configuration now is free to have better vortex shedding both into and out of the cavity as evidently seen in Figure 6. More interestingly, even though the 4-neck configuration has increased the total neck area-to-cavity volume by four times, it still appears to be effective in suppressing the same $300Hz$ signal. This finding is in contrast to the conventional theory of Helmholtz resonator where the resonance frequency is proportional to the neck area-to-cavity volume. More multi-neck configurations will have to be analysed to confirm this finding but is not pursued in this paper due to time constraint. Additionally, no conclusions could be drawn at this point of time on the effects of higher turbulence seen inside the 4-neck cavity configuration (see Figure 6) on the reduction of acoustic amplitudes presented in Table 1.

Figure 7 Low- (top, thick lines) and high-frequency (bottom, thin lines) profiles of the normalized vertical velocity component (v) in the 4-neck cavity configuration for the upstream (blue lines) and downstream necks (red lines).

5 Conclusion

In this work, a simulation setup utilizing the Lattice Boltzmann method (LBM) is described and used to simulate an impedance tube with Helmholtz cavity-backed acoustic liners. The simulation results, particularly the amplification of the applied acoustic source in a 1-neck cavity and reduction on a 4-neck cavity is corroborated by experimental results. LBM, being a highly parallelizable computational method, is then able to generate high-resolution simulation results where visualization can be undertaken to discuss the circumstances to which this amplification/reduction difference occurs. Instantaneous velocity plots presented in this paper are able to suggest some justifications. The ability for the 4-neck cavity configuration to achieve a greater acoustical reduction is likely due to a more distinct vortex shedding from the necks. This is believed to arise from the additional necks which provide an avenue for flow to enter the cavity through the downstream necks while the vortex shedding is taking place at the upstream necks, hence, resulting in greater acoustical dissipation through these stronger vortices. Even so, the visualization raises additional questions regarding the workings of a multi-neck cavity in achieving acoustical reductions. In the current work, it is seen that the utilization of the 4-neck cavity results in a higher level of turbulence within the cavity. However, it is not known if this additional turbulence would contribute to the attenuation of acoustic pressure. Addressing these matters requires more detailed analysis and might require longer simulations to be performed and are, therefore, candidates for future studies. Additional experimental work involving an optically transparent impedance tube with methods such as particle image velocimetry can also be conducted to validate the current set of simulation results presented.

References

Eldredge, J. D., & Dowling, A. P. (2003). The absorption of axial acoustic waves by a perforated liner with bias flow. *Journal of Fluid Mechanics, 485*, 307-335.

Gehrke, M., Janßen, C., & Rung, T. (2017). Scrutinizing lattice Boltzmann methods for direct numerical simulations of turbulent channel flows. *Computers & Fluids, 156*, 247-263.

Jing, X., & Sun, X. (2000). Effect of plate thickness on impedance of perforated plates with bias flow. *AIAA journal, 38*(9), 1573-1578.

Kinsler, L. E., Frey, A. R., Coppens, A. B., & Sanders, J. V. (1999). Fundamentals of acoustics. *Fundamentals of Acoustics, 4th Edition, by Lawrence E. Kinsler, Austin R. Frey, Alan B. Coppens, James V. Sanders, pp. 560. ISBN 0-471-84789-5. Wiley-VCH, December 1999.*, 560.

Krüger, T., Kusumaatmaja, H., Kuzmin, A., Shardt, O., Silva, G., & Viggen, E. M. (2017). *The Lattice Boltzmann Method: Principles and Practice*: Springer.

Ma, R., Slaboch, P. E., & Morris, S. C. (2009). Fluid mechanics of the flow-excited Helmholtz resonator. *Journal of Fluid Mechanics, 623*, 1-26.

Meyer, E., Mechel, F., & Kurtze, G. (1958). Experiments on the influence of flow on sound attenuation in absorbing ducts. *The Journal of the Acoustical Society of America, 30*(3), 165-174.

Stein, L., Reiss, J., & Sesterhenn, J. (2018). Numerical simulation of a resonant cavity: Acoustical response under grazing turbulent flow. In *New Results in Numerical and Experimental Fluid Mechanics XI* (pp. 671-681): Springer.

Sukop, M. C., & Daniel T. Thorne, J. (2006). *Lattice Boltzmann Modeling An Introduction for Geoscientists and Engineers*.

Tam, C. K., Pastouchenko, N. N., Jones, M. G., & Watson, W. R. (2014). Experimental validation of numerical simulations for an acoustic liner in grazing flow: self-noise and added drag. *Journal of Sound and Vibration, 333*(13), 2831-2854.

Viggen, E. M. (2009). *The lattice Boltzmann method with applications in acoustics*. Norwegian University of Science and Technology, Department of Physics,

Zhao, D., Ang, L., & Ji, C. (2015). Numerical and experimental investigation of the acoustic damping effect of single-layer perforated liners with joint bias-grazing flow. *Journal of Sound and Vibration, 342*, 152-167.

Fig1

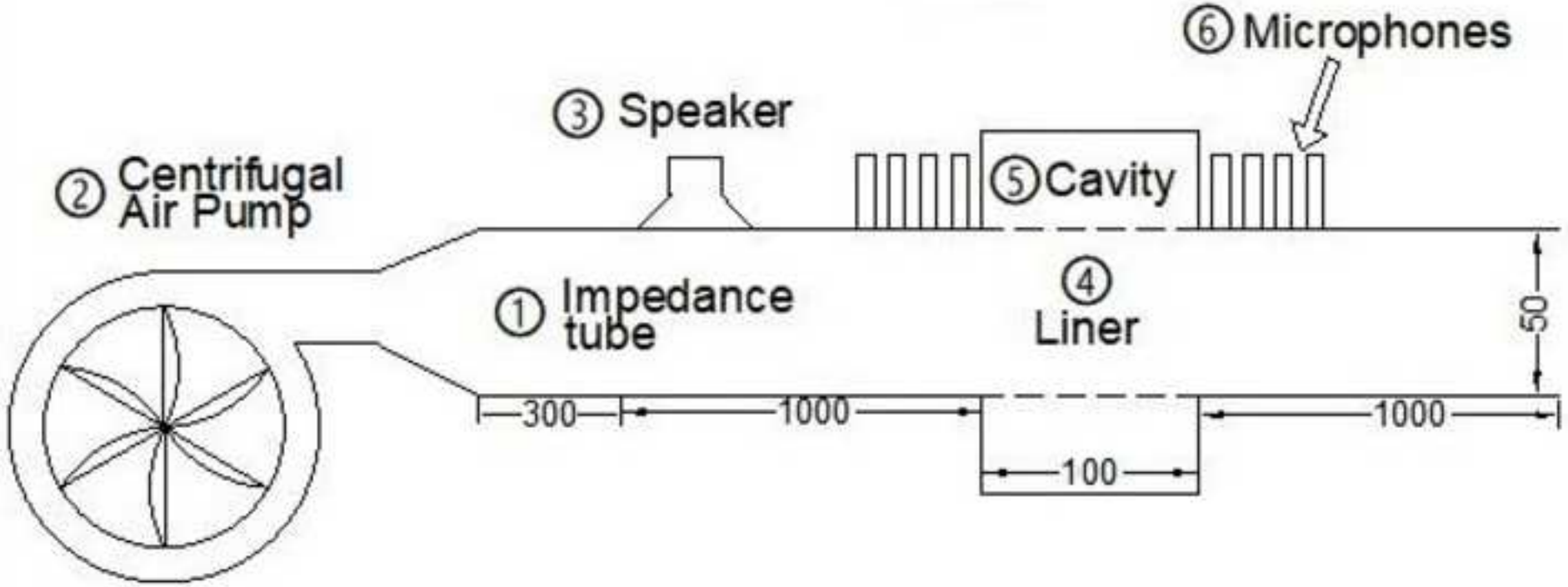

Fig2

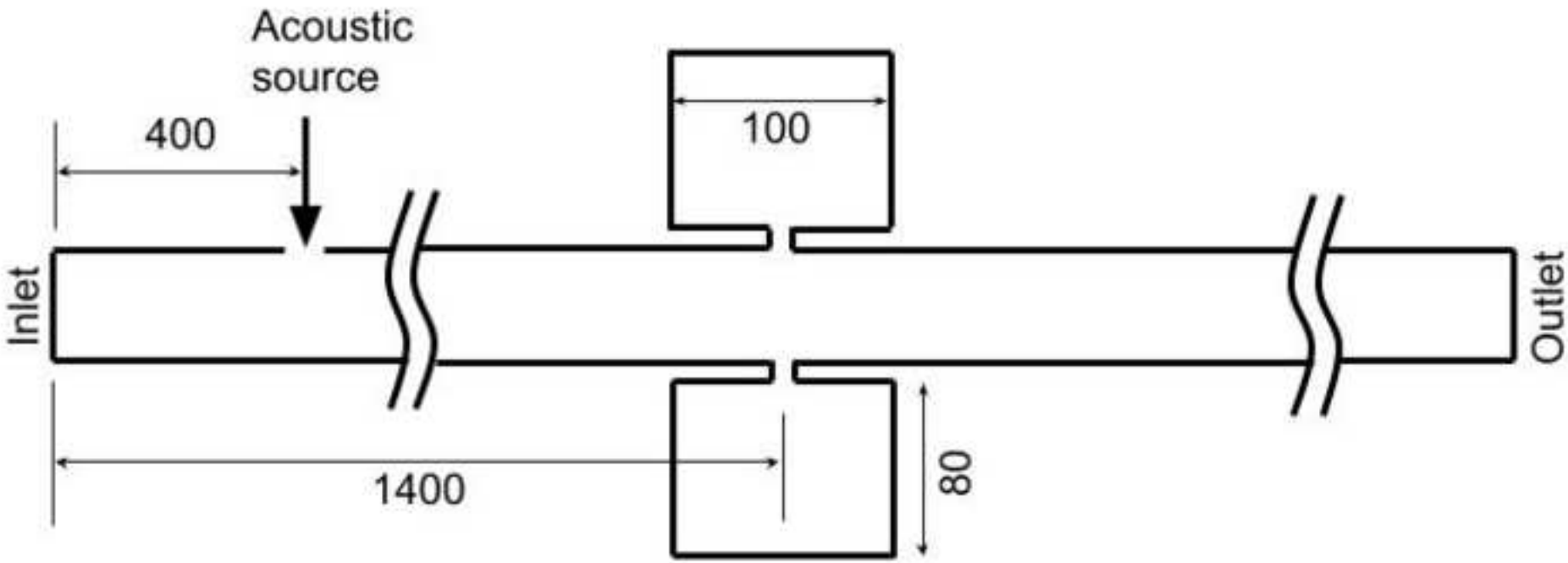

Fig3

Click here to access/download;Figure;Fig3.tif

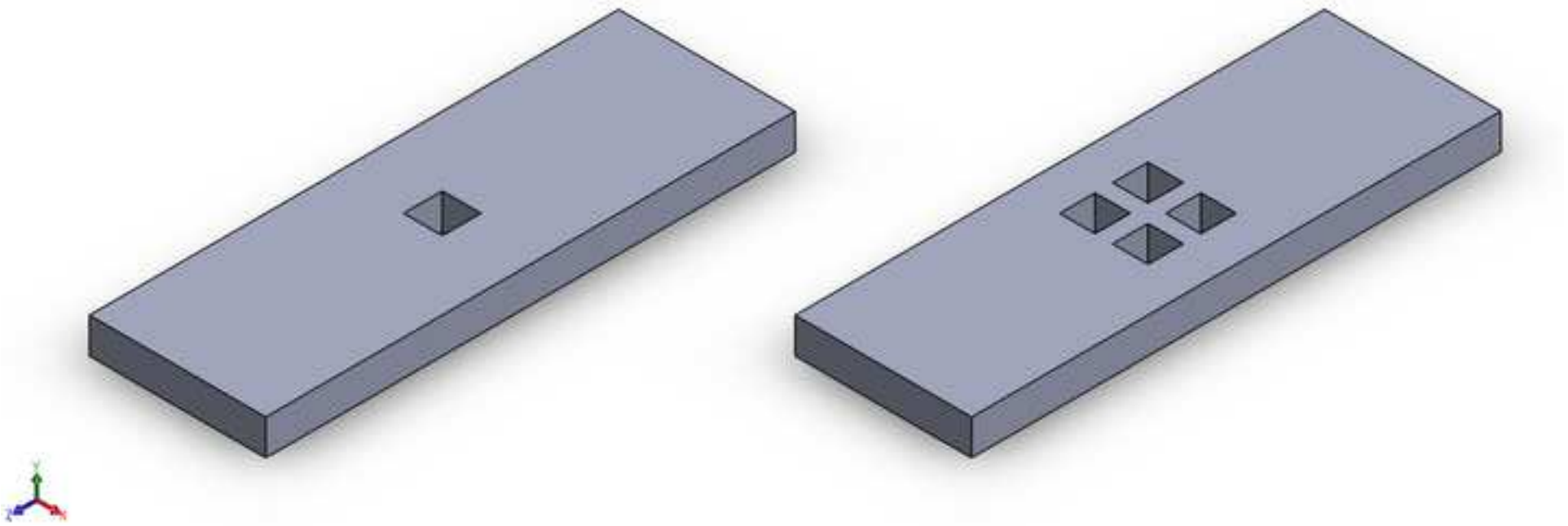

Fig4

Click here to access/download;Figure;Fig4.tif

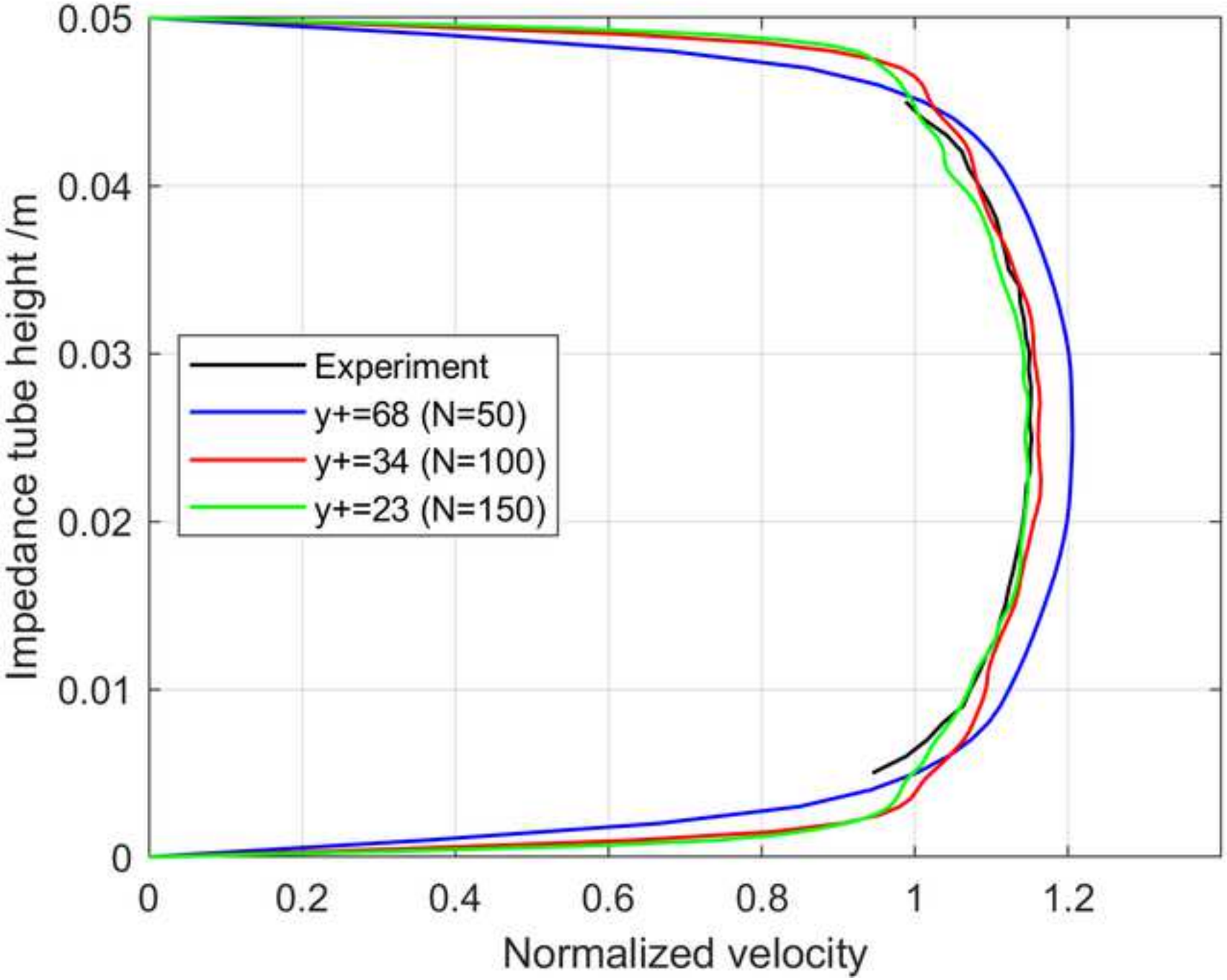

Fig5

Click here to access/download;Figure;Fig5.png

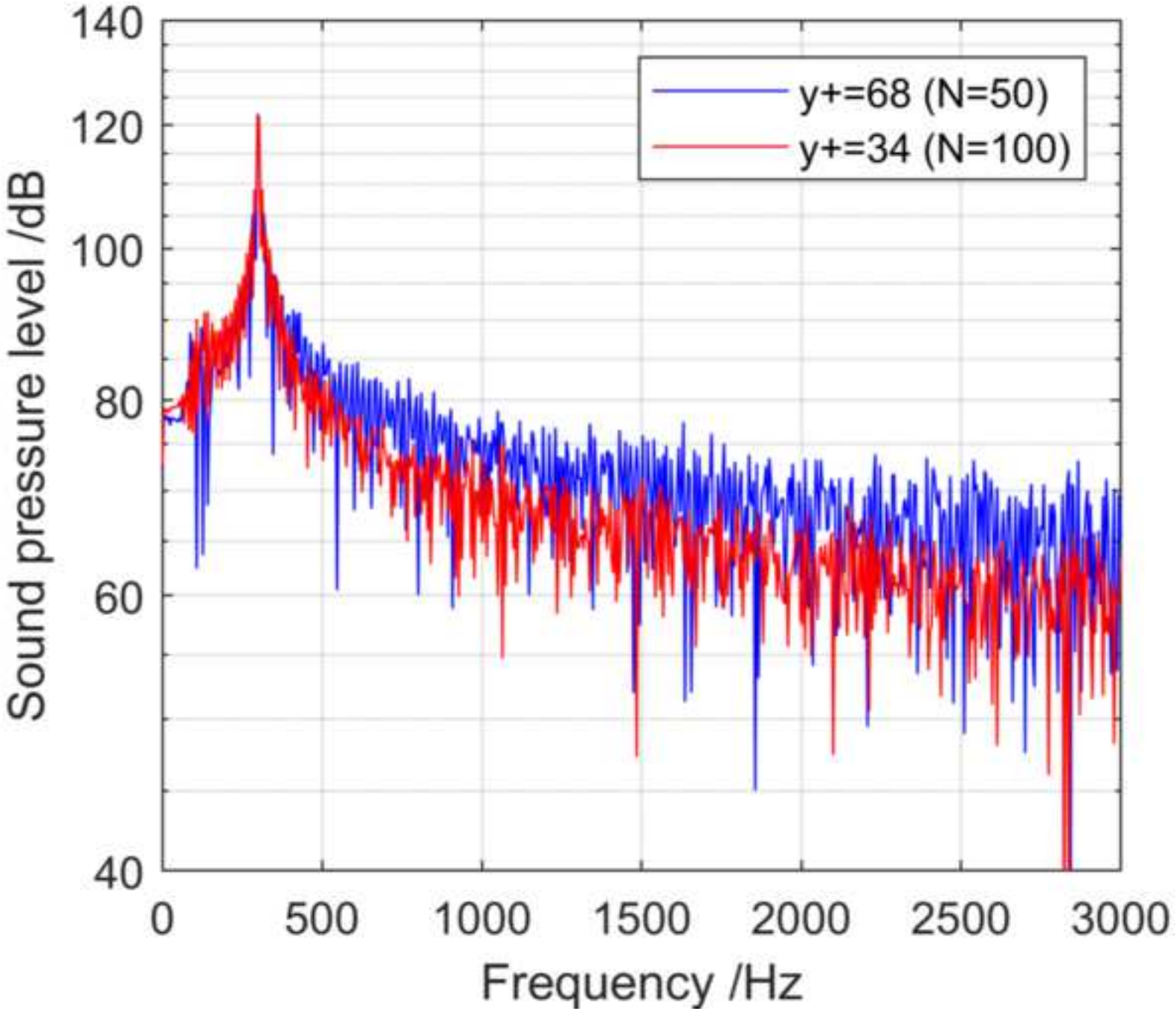

Fig6

Click here to access/download;Figure;Fig6.png

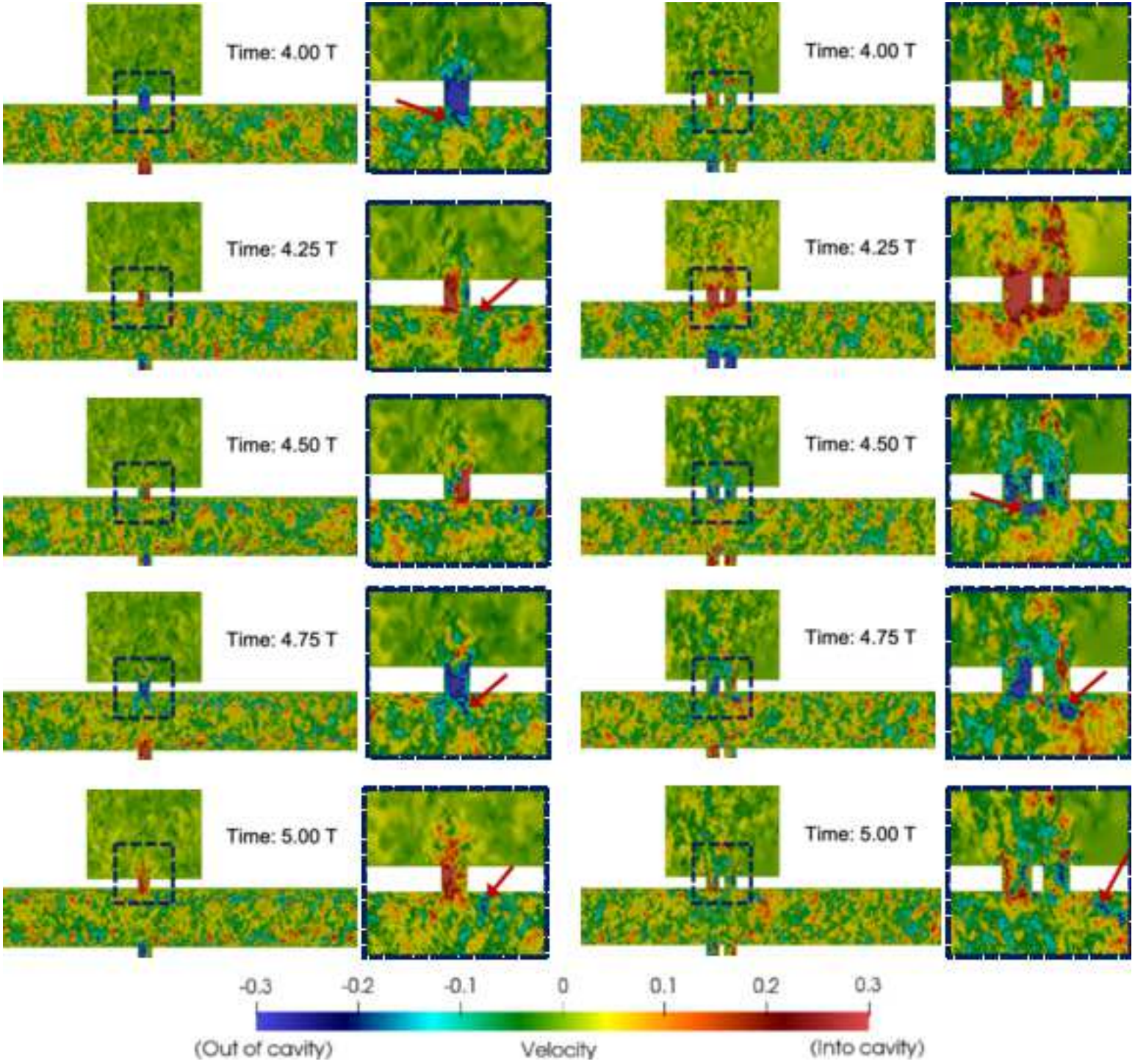

Fig7

Click here to access/download;Figure;Fig7.png

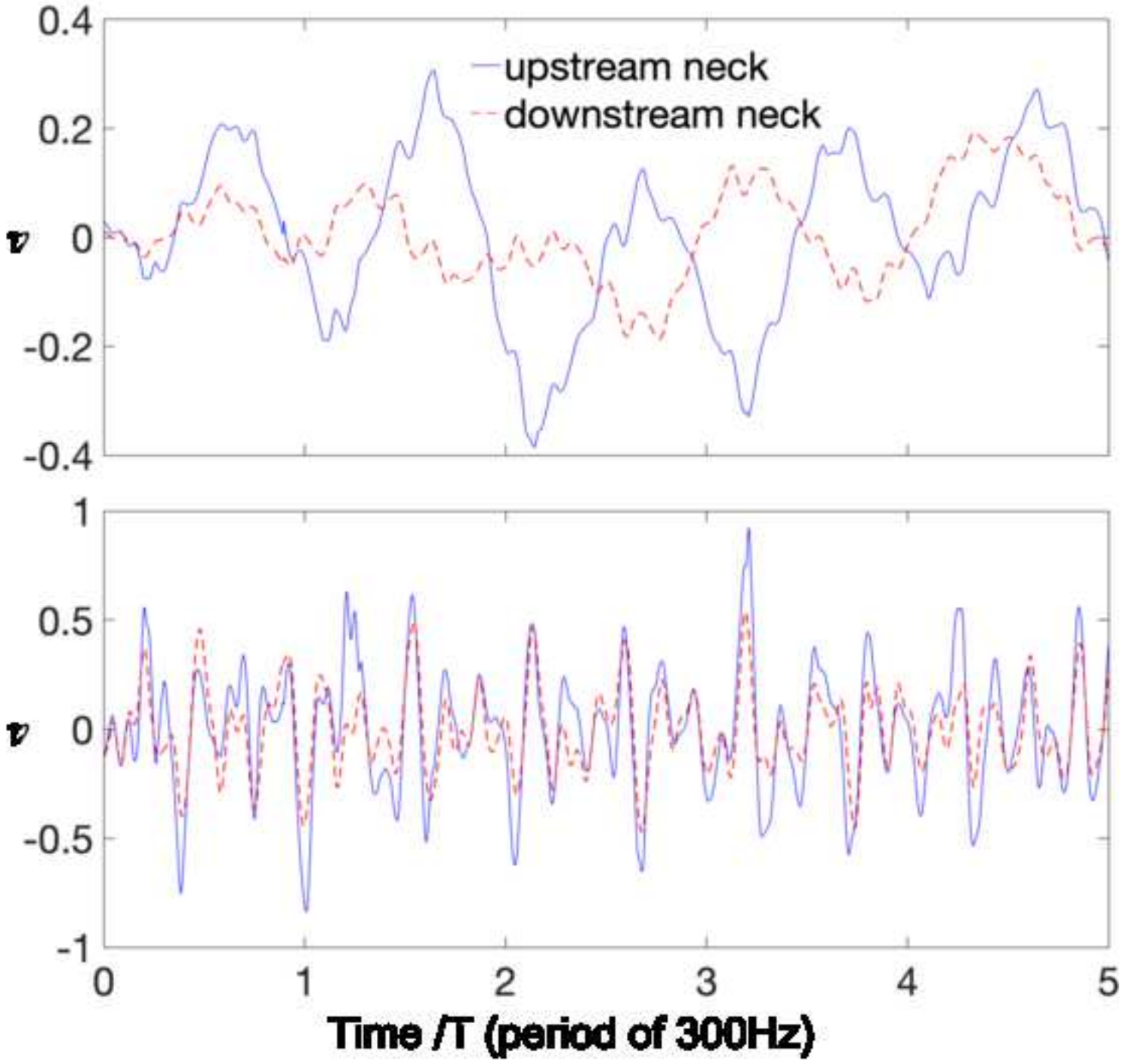

Table

Table 1 Normalized acoustic pressure of the 300Hz tone downstream of the liner

	1-neck cavity	4-neck cavity
Numerical simulation	1.488	0.767
Experiment	1.271	0.545

Click here to access/download
Supplementary Material
Media1.mp4

Click here to access/download
Supplementary Material
Media2.mp4